Chapter 5:
A Robust Upwind Discretization Method for Advection, Diffusion and Source Terms*

Barry Koren
CWI
P.O. Box 4079, 1009 AB Amsterdam, The Netherlands

5.1 Introduction

Over the past 40 years, the speed of computers has increased roughly by one order of magnitude per decade. During the next decade, continuing progress, particularly in parallel computer architectures, is expected to further raise this by three orders of magnitude. A question is whether future numerical methods for solving fluid flow problems will be capable of profiting from tomorrow's computer power. The main property of numerical methods in this respect is good robustness, particularly in complex computations which are beyond the capabilities of users, controlling computations by tuning parameters. It is mainly for their robustness that *upwind* space discretization methods have gained such a popularity. In this chapter a study is made of a robust upwind discretization technique for the scalar advection-diffusion equation (1.1), rewritten here in the 2-D form

$$\frac{\partial c}{\partial t} + \frac{\partial f(c)}{\partial x} + \frac{\partial g(c)}{\partial y} - D\left(\frac{\partial^2 c}{\partial x^2} + \frac{\partial^2 c}{\partial y^2}\right) = S(x,y). \tag{5.1}$$

The treatment of the time operator $\frac{\partial}{\partial t}$ is not of particular interest; throughout the chapter we apply the method of lines with a sufficiently accurate time integration scheme and sufficiently small time steps, such that time discretization errors are negligible with respect to space discretization errors.

In most fluid flows, advection dominates diffusion. As a consequence, when investigating space discretizations for equations of type (5.1), in the first instance it is useful to refrain from taking D as a finite parameter, but - instead - to appropriately fix it at zero. Likewise, it is also useful to first set the source term $S(x,y)$ to zero. This leads to the scalar, 2-D advection equation

$$\frac{\partial c}{\partial t} + \frac{\partial f(c)}{\partial x} + \frac{\partial g(c)}{\partial y} = 0, \tag{5.2}$$

which is less intricate than (5.1), but has the major mathematical difficulties in it. An additional advantage of the pure advection equation as a platform for developing numerical methods for more complete fluid flow equations is the ampler availability of exact reference results.

*This work was performed as part of CWI's and RIVM's EUSMOG-project.

By going from (5.1) to (5.2), solutions with layers of finite thickness have been 'simplified' to solutions with layers shrunk to zero thickness: discontinuities. Since at discontinuities, differential equations are not valid, pure advection equations require a more general concept of valid solutions than advection-diffusion equations. For this purpose, following Lax [9], instead of the differential form (5.2), we consider the integral form

$$\int\int \frac{\partial c}{\partial t} dx dy + \oint \left(f(c) n_x + g(c) n_y \right) ds = 0, \tag{5.3}$$

with n_x and n_y the components of the outward unit normal.

In fluid flows, wave motions are present which have directional preference; information is carried in various specific directions by various mechanisms. In upwind discretization methods it is tried to mimic this; upwind schemes do not allow waves to propagate equally in all directions. Furthermore, upwind discretizations of the advection equation in its integral form are shock capturing. A comment sometimes made is that near discontinuities, shock capturing schemes are very natural and useful, but that in smooth flow regions they carry around a lot of useless baggage. In our opinion, most shock capturing schemes also try to respect smooth physics; they are not just useful schemes for capturing discontinuities. Moreover, they are not that very expensive as is sometimes believed.

The upwind advection scheme to be presented in Section 5.2, is shock capturing, between second- and third-order accurate (for sufficiently smooth problems, of course), monotone in the sense of Sweby [18] in 1-D, and monotone in the sense of Spekreijse [16] in 2-D. As mentioned in Chapter 1, a property of higher than first-order accurate monotone schemes which makes these essentially different from e.g. the upwind schemes considered in Chapter 3 is that they are nonlinear, even in case of linear advection. (As is known, this nonlinearity is explained by Godunov's theorem [2], which states that no linear advection scheme exists which is both higher than first-order accurate and monotone.) In Section 5.2, a novel monotonicity (limiter) function is presented, and tested on the Problems 3.1, 3.2 and 4 (see Chapter 1 for problem definitions).

In Section 5.3, for diffusion, a standard discretization is considered. In combination with the aforementioned, limited advection scheme, it is applied to Problem 1.

In Section 5.4, for source terms, a discretization is proposed which is consistent with the discretization of the advection operator. This consistency formally is a necessity for convergence to steady state in case of zero diffusion ($D = 0$). Further, it may allow for reduction of discretization errors caused by the numerical advection operator. The discretization is investigated for Problem 2.

Throughout this chapter, for the discretization of the integral form of (5.1), we apply a cell-centered finite-volume technique. (Finite volumes allow direct satisfaction of conservation properties; cell-centering automatically leads to the natural situation that cell faces and domain boundaries coincide.) In all accuracy analyses and comparisons with exact solutions to be performed in the present chapter, for simplicity, cell-center data will be considered as point values and *not* as cell averages.

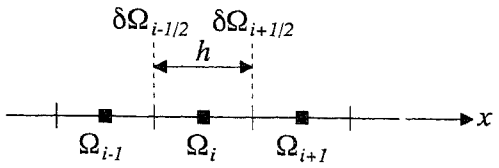

Figure 5.1: Cell-centered finite volume Ω_i with nearest neighbors

5.2 Advection

5.2.1 Accuracy in 1-D

In 1-D, a cell-centered finite-volume discretization of (5.3) yields the semi-discrete equation

$$\int_{\Omega_i} \frac{\partial c}{\partial t} dx + \left((f(c))_{i+\frac{1}{2}} - (f(c))_{i-\frac{1}{2}} \right) = 0. \tag{5.4}$$

In here, the half-integer indices $i - \frac{1}{2}$ and $i + \frac{1}{2}$ refer to the cell faces $\partial\Omega_{i-\frac{1}{2}}$ and $\partial\Omega_{i+\frac{1}{2}}$ between the (full-integer indexed) cell centers Ω_{i-1}, Ω_i and Ω_i, Ω_{i+1}, respectively (Figure 5.1). The accuracy of finite-volume discretizations is mainly determined by the way in which the cell-face fluxes are computed. Assuming that the flow is in positive x-direction, with the first-order accurate upwind scheme one takes

$$f_{i+\frac{1}{2}} = f_i. \tag{5.5}$$

Higher-order accuracy is easily obtained by piecewise polynomial interpolation. One can take for instance:

$$f_{i+\frac{1}{2}} = f_i + \frac{1+\kappa}{4}(f_{i+1} - f_i) + \frac{1-\kappa}{4}(f_i - f_{i-1}), \quad \kappa \in [-1, 1]. \tag{5.6a}$$

In here, κ is a parameter that has to be chosen from the indicated range. For $\kappa = -1$, one gets the second-order accurate, fully one-sided upwind scheme, and for $\kappa = 1$ the standard, second-order accurate central scheme. For all other values of $\kappa \in [-1, 1]$, a weighted blend is obtained between the central scheme and the fully one-sided upwind scheme. The κ-interpolation is standard and well-proven; it originates from Van Leer [10]. In case the flux function $f(c)$ is linear, instead of (5.6a), it is equivalent to take

$$f_{i+\frac{1}{2}} = f\left(c_i + \frac{1+\kappa}{4}(c_{i+1} - c_i) + \frac{1-\kappa}{4}(c_i - c_{i-1}) \right), \quad \kappa \in [-1, 1]. \tag{5.6b}$$

The first approach, (5.6a), is called *flux* interpolation; the second, (5.6b), *state* (i.e. solution) interpolation. We proceed by analyzing the precise order of accuracy of both interpolations.

Interpolating $f_{i-\frac{1}{2}}$ similar to $f_{i+\frac{1}{2}}$, substituting the polynomial expressions into (5.4), and applying truncated Taylor-series expansions (in which - as mentioned - the state values c_i are considered as point values and not as cell averages), the following modified equations are found for flux and state interpolation, respectively:

$$\frac{\partial c}{\partial t} + \frac{\partial f(c)}{\partial x} + \frac{1}{24}h^2 \frac{\partial^3 c}{\partial t \partial x^2} + \frac{\kappa - \frac{1}{3}}{4} h^2 \left(\frac{df(c)}{dc}\frac{\partial^3 c}{\partial x^3} + 3\frac{d^2 f(c)}{dc^2}\frac{\partial c}{\partial x}\frac{\partial^2 c}{\partial x^2} + \frac{d^3 f(c)}{dc^3}\left(\frac{\partial c}{\partial x}\right)^3 \right) = \mathcal{O}(h^3), \quad \kappa \in [-1, 1], \tag{5.7a}$$

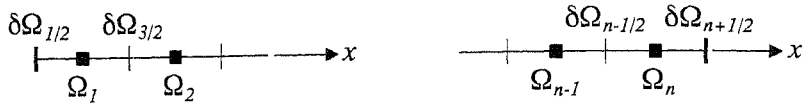

a. At inflow. b. At Outflow.

Figure 5.2: Cell-centered finite volumes near boundaries

$$\frac{\partial c}{\partial t}+\frac{\partial f(c)}{\partial x}+\frac{1}{24}h^2\frac{\partial^3 c}{\partial t\partial x^2}+\frac{1}{4}h^2\left(\left(\kappa-\frac{1}{3}\right)\frac{df(c)}{dc}\frac{\partial^3 c}{\partial x^3}+\kappa\frac{d^2f(c)}{dc^2}\frac{\partial c}{\partial x}\frac{\partial^2 c}{\partial x^2}+\frac{1}{6}\frac{d^3f(c)}{dc^3}\left(\frac{\partial c}{\partial x}\right)^3\right)=\mathcal{O}(h^3),\quad \kappa\in[-1,1]. \tag{5.7b}$$

First note that - as should be - both modified equations are identical in case of a linear $f(c)$; for e.g.

$$f(c)=uc,\quad u=\text{constant}>0, \tag{5.8}$$

with u the velocity (which is constant because mass conservation of the fluid requires $\frac{\partial u}{\partial x}=0$), we get for both interpolations:

$$\frac{\partial c}{\partial t}+u\frac{\partial c}{\partial x}+\frac{1}{24}h^2\frac{\partial^3 c}{\partial t\partial x^2}+\frac{\kappa-\frac{1}{3}}{4}h^2u\frac{\partial^3 c}{\partial x^3}=\mathcal{O}(h^3),\quad \kappa\in[-1,1]. \tag{5.9}$$

Continuing again with (5.7a) and (5.7b), note that both flux and state interpolation lead to a second-order accurate discretization under the constraint that $f(c)$ and c are sufficiently smooth. Also note that for steady linear problems both interpolations become third-order accurate for the specific choice $\kappa=\frac{1}{3}$; flux interpolation for steady nonlinear problems as well. Among the four test problems prescribed in Chapter 1, no steady nonlinear problem prevails. In the following we restrict ourselves to state interpolation; i.e. to (5.6b). Herewith, as value for κ, we take $\kappa=\frac{1}{3}$.

A disadvantage of the piecewise polynomial interpolation of the type (5.6b), also of the type (5.6a) otherwise, is that it cannot be applied straightforward up to and including boundaries. First, consider the 1-D situation given in Figure 5.2a, in which cell face $\partial\Omega_{\frac{1}{2}}$ coincides with the inflow boundary. The flux across the inflow boundary does not need to be approximated; it is known exactly through the boundary condition. At the first inner cell face, cell face $\partial\Omega_{\frac{3}{2}}$ (where the flux *does* need to be approximated), one generally gets a consistency problem. Since Ω_{-1} does not exist (we refrain from introducing any dummy cell across boundaries), at cell face $\partial\Omega_{\frac{3}{2}}$, (5.6b) cannot be applied for all $\kappa\in[-1,1)$. Only central interpolation ($\kappa=1$) can be applied consistently here. However, at the outflow boundary (Figure 5.2b), at cell face $\partial\Omega_{n+\frac{1}{2}}$, the central scheme can *not* be applied consistently. Since there Ω_{n+1} does not exist, at $\partial\Omega_{n+\frac{1}{2}}$ it is only the fully one-sided upwind scheme ($\kappa=-1$), that can be applied consistently. A higher-order accurate scheme exists which is consistent at both inflow and outflow boundaries: the superbox scheme [3, 4]. It is a scheme which properly alternates between central ($\kappa=1$) and fully one-sided upwind ($\kappa=-1$) at all consecutive cell faces, with as the merit: consistency

up to and including all boundaries, but with as a drawback: a slightly reduced accuracy in comparison to the uniform κ-schemes. Here we do not apply the superbox scheme and accept the boundary-inconsistency of the κ-schemes. At $\partial\Omega_{\frac{3}{2}}$ we apply the $\kappa = 1$-scheme and at $\partial\Omega_{n+\frac{1}{2}}$ the $\kappa = -1$-scheme. With $\kappa = \frac{1}{3}$ applied at all other, interior cell faces, this gives a local reduction to first-order accuracy in the cells Ω_1, Ω_2 and Ω_n. We demonstrate this for the simple flux function (5.8). For this flux function, in Ω_1, Ω_2 and Ω_n one has to satisfy, respectively

$$\int_{\Omega_1} \frac{\partial c}{\partial t} dx + u\left(c_{\frac{3}{2}} - c_{\frac{1}{2}}\right) = 0, \tag{5.10a}$$

$$\int_{\Omega_2} \frac{\partial c}{\partial t} dx + u\left(c_{\frac{5}{2}} - c_{\frac{3}{2}}\right) = 0, \tag{5.10b}$$

$$\int_{\Omega_n} \frac{\partial c}{\partial t} dx + u\left(c_{n+\frac{1}{2}} - c_{n-\frac{1}{2}}\right) = 0. \tag{5.10c}$$

Applying Taylor-series expansions after having substituted: the boundary condition relation

$$c_{\frac{1}{2}} = c_{\text{in}}, \tag{5.11a}$$

the $\kappa = 1$-relation

$$c_{\frac{3}{2}} = \frac{1}{2}\left(c_1 + c_2\right), \tag{5.11b}$$

the $\kappa = \frac{1}{3}$-relations

$$c_{\frac{5}{2}} = c_2 + \frac{1}{3}\left(c_3 - c_2\right) + \frac{1}{6}\left(c_2 - c_1\right), \tag{5.11c}$$

$$c_{n-\frac{1}{2}} = c_{n-1} + \frac{1}{3}\left(c_n - c_{n-1}\right) + \frac{1}{6}\left(c_{n-1} - c_{n-2}\right), \tag{5.11d}$$

and the $\kappa = -1$-relation

$$c_{n+\frac{1}{2}} = c_n + \frac{1}{2}\left(c_n - c_{n-1}\right), \tag{5.11e}$$

from (5.10a)-(5.10c) we derive the corresponding modified equations

$$\left(\frac{\partial c}{\partial t} + u\frac{\partial c}{\partial x} + \frac{h}{8}u\frac{\partial^2 c}{\partial x^2}\right)_1 = \mathcal{O}(h^2), \tag{5.12a}$$

$$\left(\frac{\partial c}{\partial t} + u\frac{\partial c}{\partial x} - \frac{h}{6}u\frac{\partial^2 c}{\partial x^2}\right)_2 = \mathcal{O}(h^2), \tag{5.12b}$$

$$\left(\frac{\partial c}{\partial t} + u\frac{\partial c}{\partial x} - \frac{h}{3}u\frac{\partial^2 c}{\partial x^2}\right)_n = \mathcal{O}(h^2), \tag{5.12c}$$

which all three show a reduction to first-order accuracy indeed. A peculiarity of modified equation (5.12a) is that it contains an anti-diffusion term. In case of e.g. a solution layer at the inflow boundary, one needs to be aware of this; it may give rise to local instability. The local first-order accuracies in Ω_1, Ω_2 and Ω_n will not reduce global second-order solution accuracy, measured in L_1-norm.

5.2.2 Monotonicity in 1-D

We still have to pay attention to the aspect of monotonicity, i.e. to the possible occurrence of wiggles and their suppression, as well as to the possible occurrence of negative solution values and their suppression. (As mentioned in Chapter 1: in the computational modeling of e.g. air-pollutant transport with chemical reactions, the requirement of solution positivity is a prerequisite for stability of the chemical reaction computations.) To assure positivity of solutions, a discretization should be sufficiently conservative *and* monotone.

To investigate monotonicity, for reasons of transparency, we consider the steady, 1-D, linear advection operator with for $f(c)$ again (5.8). Then, the discrete advection operator simply reads

$$u(c_{i+\frac{1}{2}} - c_{i-\frac{1}{2}}). \tag{5.13}$$

Applying the κ-scheme in interpolating $c_{i-\frac{1}{2}}$ and $c_{i+\frac{1}{2}}$, (5.13) can be rewritten in the stencil form

$$u \left[\begin{array}{cccc} \frac{1-\kappa}{4} c_{i-2} & \frac{-5+3\kappa}{4} c_{i-1} & \frac{3(1-\kappa)}{4} c_i & \frac{1+\kappa}{4} c_{i+1} \end{array} \right], \quad \kappa \in [-1, 1]. \tag{5.14}$$

Verify that no value of $\kappa \in [-1, 1]$ exists for which the positive coefficients rule [6, 12] is satisfied. Schemes which do not obey this rule admit spurious solution oscillations. The worst κ-scheme with respect to the positive coefficients rule is the $\kappa = 1$-scheme: the standard, second-order accurate, central scheme.

We proceed by making the $\kappa = \frac{1}{3}$-scheme monotone. We do so by following Sweby's monotonicity theory [18], which is based on a monitor that considers a ratio of consecutive solution gradients per cell face. Then, the limited cell-face state $c_{i+\frac{1}{2}}$ reads

$$c_{i+\frac{1}{2}} = c_i + \frac{1}{2}\phi(r_{i+\frac{1}{2}})(c_i - c_{i-1}). \tag{5.15a}$$

In here, $\phi = \phi(r)$ is the limiter function, which must be inside (or at the boundary of) Sweby's monotonicity domain. Accuracy requires that $\phi(1) = 1$. In (5.15a), the limiter argument $r_{i+\frac{1}{2}}$ is the upwind ratio of consecutive solution gradients:

$$r_{i+\frac{1}{2}} \equiv \frac{c_{i+1} - c_i + \epsilon}{c_i - c_{i-1} + \epsilon}, \tag{5.15b}$$

with ϵ some very small number (e.g. $\epsilon = 10^{-10}$), introduced to avoid, e.g., division by zero in uniform flow regions.

Verify that the non-limited $\kappa = \frac{1}{3}$-scheme can be written analogously to (5.15a) as

$$c_{i+\frac{1}{2}} = c_i + \frac{1}{2}\left(\frac{1}{3} + \frac{2}{3} r_{i+\frac{1}{2}}\right)(c_i - c_{i-1}). \tag{5.16}$$

In Figure 5.3, the non-limited $\kappa = \frac{1}{3}$-scheme has been indicated by the oblique dashed line; for $r < \frac{1}{4}$ and $r > \frac{5}{2}$ it is out of the monotonicity domain. It can be directly seen that the limiter function which is most consistent with the non-limited $\kappa = \frac{1}{3}$-scheme and which obeys the present monotonicity rules, reads:

$$\phi(r) = \max\left(0, \min\left(2r, \min\left(\frac{1}{3} + \frac{2}{3}r, 2\right)\right)\right). \tag{5.17}$$

This novel $\kappa = \frac{1}{3}$-limiter (depicted by the thick solid line in Figure 5.3) differs significantly from the $\kappa = \frac{1}{3}$-limiter presented in [5]. Whereas the earlier limiter from [5] is

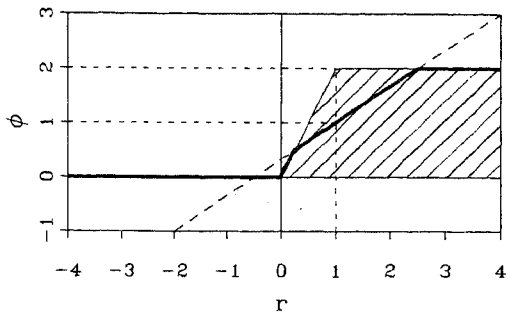

Figure 5.3: Limiter $\phi(r) = \max\left(0, \min\left(2r, \min\left(\frac{1}{3} + \frac{2}{3}r, 2\right)\right)\right)$ and Sweby's monotonicity domain

differentiable, the present limiter (5.17) is not. Since differentiability will not be required, here we have chosen for the best resemblance between the non-limited target scheme and the limited scheme, in order to have the best possible accuracy. (The present limited $\kappa = \frac{1}{3}$-scheme is tangent to the non-limited $\kappa = \frac{1}{3}$-scheme over the entire r-range $(\frac{1}{4}, \frac{5}{2})$; the earlier limited $\kappa = \frac{1}{3}$-scheme from [5] only at $r = 1$.) For formal evidences on accuracy and monotonicity in 1-D, we refer to [18]; that theory is not repeated here.

Like the non-limited $\kappa = \frac{1}{3}$-scheme, a limited $\kappa = \frac{1}{3}$-scheme also cannot be applied consistently near boundaries. There we apply again (5.11a), (5.11b) and (5.11e). None of the corresponding discrete equations is positive; in Ω_1, Ω_2 and Ω_n we have as stencils, respectively:

$$u\left[\begin{array}{ccc} -c_{\text{in}} & \frac{1}{2}c_1 & \frac{1}{2}c_2 \end{array}\right], \tag{5.18a}$$

$$u\left[\begin{array}{ccc} -\frac{2}{3}c_1 & \frac{1}{3}c_2 & \frac{1}{3}c_3 \end{array}\right], \tag{5.18b}$$

$$u\left[\begin{array}{ccc} \frac{1}{6}c_{n-2} & -\frac{4}{3}c_{n-1} & -\frac{7}{6}c_n \end{array}\right]. \tag{5.18c}$$

Since there is no boundary-layer problem among the set of four prescribed test problems, a fix to this deficiency is probably not necessary.

Still a general difficulty of limited discretizations is that when dealing with unsteady problems, formally, the aspect of monotonicity as just investigated for space operator (5.13) should be further investigated for its unsteady extension. Some rigorous numerical analyses have already been performed in this respect (see e.g. [1, 8, 14, 15, 17]). A general conclusion that can be drawn from these analyses is that to avoid non-monotonicity, one should not only have a positive space discretization, but also a sufficiently small time step. (Hence, besides for stability and accuracy, the time step should also be sufficiently small for monotonicity.) Here we refrain from analyzing monotonicity in an unsteady context; in all unsteady experiments to be considered hereafter, the time steps will already be small for accuracy reasons.

5.2.3 Discretization in 2-D

No attempt is made to apply here a monotone, second-order accurate, 'genuinely' multi-D upwind scheme, as we did in e.g. [7]. For the application of 'genuinely' multi-D upwind schemes in the present book, we refer to Chapters 3 and 11. In this chapter, striving for

a robust discretization, we just follow the directionally-split, grid-aligned, 1-D upwind approach, with as the 1-D upwind scheme: the limited $\kappa = \frac{1}{3}$-scheme (with state interpolation), as just discussed and applied. With the velocity field given as a continuous function, in multi-D, state interpolation has the advantage over flux interpolation that it allows an exact evaluation of velocities at cell faces. The previous accuracy properties directly carry over from 1-D to 2-D. With Spekreijse's 2-D extension of Sweby's monotonicity theory, the monotonicity properties also carry over from 1-D to 2-D. Theoretical evidence for this is not repeated here. Considering e.g. the flux functions $f(c) = uc$ and $g(c) = vc$, with the x- and y-velocity components $u = u(x, y)$ and $v = v(x, y)$ defined in the entire computational domain, and with the i- and j-directions in the same directions as the x- and y-axes (Figure 5.4), the present 2-D, limited $\kappa = \frac{1}{3}$-scheme reads as follows; at the vertical cell faces:

if $u_{i+\frac{1}{2},j} \geq 0$:

$$\begin{array}{ll}
\text{if } i = 0: & (f(c))_{\frac{1}{2},j} = (u_{\text{in}})_j (c_{\text{in}})_j, \\
\text{if } i = 1: & (f(c))_{\frac{3}{2},j} = u_{\frac{3}{2},j} \frac{1}{2}(c_{1,j} + c_{2,j}), \\
\text{if } i = n: & (f(c))_{n+\frac{1}{2},j} = u_{n+\frac{1}{2},j} \left(c_{n,j} + \frac{1}{2}(c_{n,j} - c_{n-1,j}) \right), \\
\text{else}: & (f(c))_{i+\frac{1}{2},j} = u_{i+\frac{1}{2},j} \left(c_{i,j} + \frac{1}{2}\phi(r_{i+\frac{1}{2},j})(c_{i,j} - c_{i-1,j}) \right), \\
& r_{i+\frac{1}{2},j} = \frac{c_{i+1,j} - c_{i,j} + \epsilon}{c_{i,j} - c_{i-1,j} + \epsilon},
\end{array} \tag{5.19a}$$

else :

$$\begin{array}{ll}
\text{if } i = 0: & (f(c))_{\frac{1}{2},j} = u_{\frac{1}{2},j} \left(c_{1,j} + \frac{1}{2}(c_{1,j} - c_{2,j}) \right), \\
\text{if } i = n-1: & (f(c))_{n-\frac{1}{2},j} = u_{n-\frac{1}{2},j} \frac{1}{2}(c_{n,j} + c_{n-1,j}), \\
\text{if } i = n: & (f(c))_{n+\frac{1}{2},j} = (u_{\text{in}})_j (c_{\text{in}})_j, \\
\text{else}: & (f(c))_{i+\frac{1}{2},j} = u_{i+\frac{1}{2},j} \left(c_{i+1,j} + \frac{1}{2}\phi(r_{i+\frac{1}{2},j})(c_{i+1,j} - c_{i+2,j}) \right), \\
& r_{i+\frac{1}{2},j} = \frac{c_{i,j} - c_{i+1,j} + \epsilon}{c_{i+1,j} - c_{i+2,j} + \epsilon};
\end{array} \tag{5.19b}$$

and likewise, at the horizontal cell faces:

if $v_{i,j+\frac{1}{2}} \geq 0$:

$$\begin{array}{ll}
\text{if } j = 0: & (g(c))_{i,\frac{1}{2}} = (v_{\text{in}})_i (c_{\text{in}})_i, \\
\text{if } j = 1: & (g(c))_{i,\frac{3}{2}} = v_{i,\frac{3}{2}} \frac{1}{2}(c_{i,1} + c_{i,2}), \\
\text{if } j = n: & (g(c))_{i,n+\frac{1}{2}} = v_{i,n+\frac{1}{2}} \left(c_{i,n} + \frac{1}{2}(c_{i,n} - c_{i,n-1}) \right), \\
\text{else}: & (g(c))_{i,j+\frac{1}{2}} = v_{i,j+\frac{1}{2}} \left(c_{i,j} + \frac{1}{2}\phi(r_{i,j+\frac{1}{2}})(c_{i,j} - c_{i,j-1}) \right), \\
& r_{i,j+\frac{1}{2}} = \frac{c_{i,j+1} - c_{i,j} + \epsilon}{c_{i,j} - c_{i,j-1} + \epsilon},
\end{array} \tag{5.20a}$$

else :

$$\begin{array}{ll}
\text{if } j = 0: & (g(c))_{i,\frac{1}{2}} = v_{i,\frac{1}{2}} \left(c_{i,1} + \frac{1}{2}(c_{i,1} - c_{i,2}) \right), \\
\text{if } j = n-1: & (g(c))_{i,n-\frac{1}{2}} = v_{i,n-\frac{1}{2}} \frac{1}{2}(c_{i,n} + c_{i,n-1}), \\
\text{if } j = n: & (g(c))_{i,n+\frac{1}{2}} = (v_{\text{in}})_i (c_{\text{in}})_i, \\
\text{else}: & (g(c))_{i,j+\frac{1}{2}} = v_{i,j+\frac{1}{2}} \left(c_{i,j+1} + \frac{1}{2}\phi(r_{i,j+\frac{1}{2}})(c_{i,j+1} - c_{i,j+2}) \right), \\
& r_{i,j+\frac{1}{2}} = \frac{c_{i,j} - c_{i,j+1} + \epsilon}{c_{i,j+1} - c_{i,j+2} + \epsilon}.
\end{array} \tag{5.20b}$$

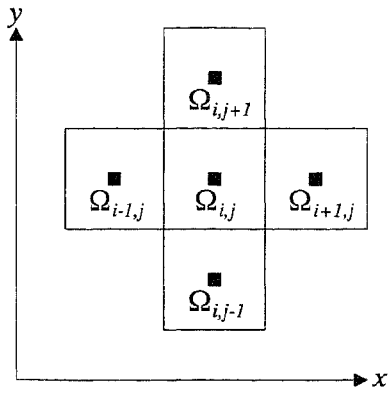

Figure 5.4: Cell-centered finite volume $\Omega_{i,j}$ with nearest neighbors

As the limiter function $\phi = \phi(r)$ we still apply (5.17). The discretization of the advective fluxes has been completely defined now, both in 1-D and 2-D. Note that it is a discretization without any tuning parameter.

5.2.4 Numerical results

To investigate the properties of this advection discretization, numerical experiments are performed for successively the Problems 3.1, 3.2 and 4. To investigate the accuracy behaviors, numerical solutions are computed on a sequence of three increasingly finer grids. Comparisons are made with the exact discrete solutions. For time integration, the explicit, fourth-order accurate, four-stage Runge-Kutta scheme is applied. The time step is taken linearly proportional to the mesh size, and sufficiently small to ensure that time discretization errors are negligible with respect to space discretization errors. (Stability and monotonicity are supposed to be guaranteed by these small time steps.) The phenomenon of order reduction of Runge-Kutta schemes as investigated in [13], is expected to play no role. In the present problems, at the inflow boundaries, c and its second derivative normal to the boundary, are very close to zero for $t > 0$.

Problem 3 For Problem 3, 1-D nonlinear advection is the issue. The flux function defined for it is

$$f(c) = c^n, \tag{5.21}$$

where in the test case specified first (Problem 3.1): $n = 2$, and in the second test case (Problem 3.2): $n = 5$. In both cases we take a sequence of grids, with successively $h = \frac{1}{10}$, $h = \frac{1}{20}$ and $h = \frac{1}{40}$. To give an indication of the computational costs of the limited scheme, flux computing times are given which are relative to those of the non-limited, standard, second-order accurate central scheme.

Problem 3.1. In Figure 5.5 we give the numerical solutions. The limited scheme yields monotone solutions on all three grids, and no (visible) phase errors. In Table 5.1, for each of the three grids, the L_1- and L_∞-norms of the solution errors ($\|\Delta c\|_1$ and $\|\Delta c\|_\infty$) are given; $\|\Delta c\|_1$ behaves in between $\mathcal{O}(h^2)$ and $\mathcal{O}(h^3)$, and $\|\Delta c\|_\infty$ in between $\mathcal{O}(h)$ and $\mathcal{O}(h^2)$. It seems that for $h \downarrow 0$, the convergence of both $\|\Delta c\|_1$ and $\|\Delta c\|_\infty$ tends to $\mathcal{O}(h^2)$. Also given in the table are: the errors in the ratio of numerical mass and exact discrete mass (integrated over the computational domain at $t = 1$). The mass errors,

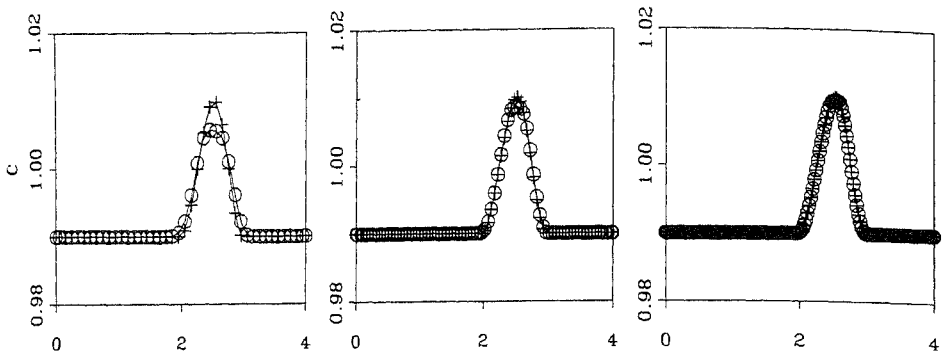

a. $h = \frac{1}{10}$. b. $h = \frac{1}{20}$. c. $h = \frac{1}{40}$.

Figure 5.5: Solutions Problem 3.1; ○ : numerical, + : exact

Table 5.1: Numerical results Problem 3.1

	$h = \frac{1}{10}$	$h = \frac{1}{20}$	$h = \frac{1}{40}$
$\|\Delta c\|_1$	52.1×10^{-5}	9.8×10^{-5}	1.9×10^{-5}
$\|\Delta c\|_\infty$	42.4×10^{-4}	14.6×10^{-4}	4.6×10^{-4}
$1 - r_{\text{mass}}$	1.0×10^{-11}	-1.3×10^{-11}	-1.1×10^{-11}
$r_{\text{CPU-time}}$	2.3	2.0	1.8

denoted by $1 - r_{\text{mass}}$, seem to be at machine zero. Further we give the ratios of CPU-time as consumed on the three grids from $t = 0$ to $t = 1$, by the limited $\kappa = \frac{1}{3}$-scheme and the standard, second-order central scheme. The h-dependency of the CPU-time ratios, denoted by $r_{\text{CPU-time}}$, is supposed to be caused by differences in computational overhead of the limited $\kappa = \frac{1}{3}$-scheme and the standard, second-order central scheme. (The best measure for the cost ratio of both schemes is obtained on the finest mesh, $h = \frac{1}{40}$.)

Problem 3.2. Numerical results obtained for this test case are depicted in Figure 5.6. They are satisfactory; limiter (5.17) appears to do a good job. In Table 5.2, we give the values for the same quantities considered in Table 5.1. Due to the shock wave, as expected, $\|\Delta c\|_\infty$ behaves $\mathcal{O}(1)$. As a consequence, $\|\Delta c\|_1$ behaves (about) $\mathcal{O}(h)$. Probably, due to infinitely large solution derivatives, here the mass errors are above machine zero and of zeroth-order behavior. Concerning the relative computational costs; at the finest grid ($h = \frac{1}{40}$), the limited $\kappa = \frac{1}{3}$-scheme is equally expensive as for Problem 3.1: 1.8 times the standard, second-order central scheme. Probably, the CPU-time ratio 1.8 is a good measure for any 1-D advection problem.

Problem 4 For Problem 4, multi-dimensionality is the issue. It is solved on an equidistant, cell-centered finite-volume grid with successively 22×21, 42×41 and 82×81 cells, in x- and y-direction, respectively. (These dimensions allow an exact capturing of the local maximum in the initial solution.) During time integration, the exact, unsteady inflow is imposed.

In Figure 5.7 we give the iso-line distributions of the exact solutions and in Figure 5.8 the distributions obtained by the limited $\kappa = \frac{1}{3}$-scheme. In Table 5.3 some more

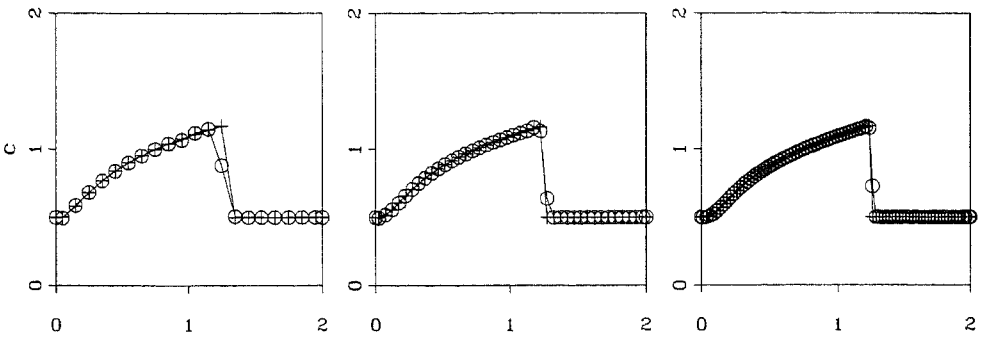

a. $h = \frac{1}{10}$. b. $h = \frac{1}{20}$. c. $h = \frac{1}{40}$.

Figure 5.6: Solutions Problem 3.2; ○: numerical, +: exact

Table 5.2: Numerical results Problem 3.2

	$h = \frac{1}{10}$	$h = \frac{1}{20}$	$h = \frac{1}{40}$
$\|\Delta c\|_1$	17.3×10^{-3}	5.0×10^{-3}	3.2×10^{-3}
$\|\Delta c\|_\infty$	2.9×10^{-1}	1.4×10^{-1}	2.3×10^{-1}
$1 - r_{\text{mass}}$	18.5×10^{-3}	-3.6×10^{-3}	-3.6×10^{-3}
$r_{\text{CPU-time}}$	1.5	1.2	1.8

information is given. The solution errors appear to behave in between $\mathcal{O}(h^2)$ and $\mathcal{O}(h^3)$ with respect to $\|\Delta c\|_1$, and in between $\mathcal{O}(h)$ and $\mathcal{O}(h^2)$ with respect to $\|\Delta c\|_\infty$. As opposed to the tendency towards an $\mathcal{O}(h^2)$-convergence of $\|\Delta c\|_1$ for Problem 3.1, here $\|\Delta c\|_1$ seems to tend to an $\mathcal{O}(h^3)$-behavior. The mass error occurring for Problem 4 is mainly caused by the fact that at the inflow boundaries, the exact fluxes are imposed, whereas at the outflow boundaries - mathematically correct - the fluxes are computed from the interior numerical solution. As a consequence, due to discretization errors, the total net flux is not zero. As expected, the mass error appears to behave more or less like $\|\Delta c\|_1$: in between $\mathcal{O}(h^2)$ and $\mathcal{O}(h^3)$. Concerning the peak error $1 - c_{\max}$, as was to be expected, it converges at about the same rate as $\|\Delta c\|_\infty$. The positivity error $c_{\min}$ shows that the numerical solutions are practically positive. Their convergence to machine zero is very fast. That these errors are not at machine zero (on all three grids) is attributed to the fact that the discretization is not positive near boundaries; see (5.18a)-(5.18c). Concerning the computational costs, in 2-D the limited $\kappa = \frac{1}{3}$-scheme seems to be 2.4 times as expensive as the standard, second-order central scheme. In 2-D, the limited $\kappa = \frac{1}{3}$-scheme is of course relatively more expensive than in 1-D because of the checking of flow directions. In addition, we also give the absolute computing times, together with the time needed for the benchmark computation (Problem 4 on a 40 × 40-grid; see Chapter 15 for further details). All four computing times in Table 5.3 have been measured on an SGI workstation, under identical compiler settings. The CPU-times of the limited $\kappa = \frac{1}{3}$-scheme tend to an $\mathcal{O}(h^{-3})$-behavior, which is explained by the linear dependence of the time step on the mesh size.

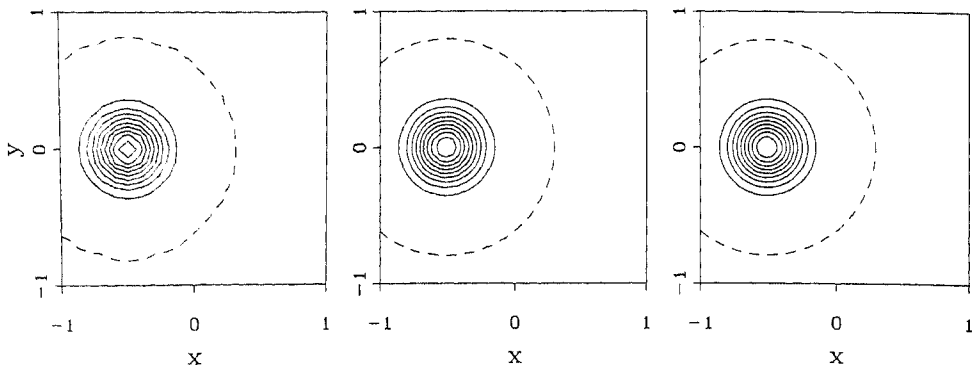

a. 22 × 21-grid. b. 42 × 41-grid. c. 82 × 81-grid.

Figure 5.7: Exact solutions Problem 4

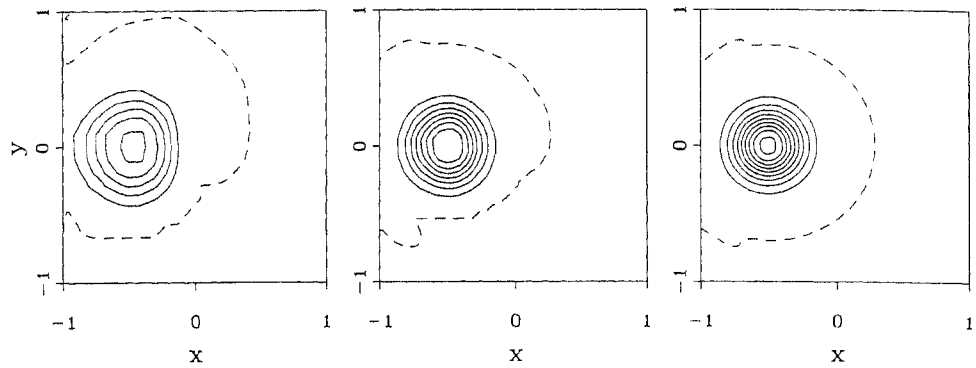

a. 22 × 21-grid. b. 42 × 41-grid. c. 82 × 81-grid.

Figure 5.8: Numerical solutions Problem 4

Table 5.3: Numerical results Problem 4

	22 × 21-grid	42 × 41-grid	82 × 81-grid
$\|\Delta c\|_1$	157.1×10^{-4}	45.2×10^{-4}	7.3×10^{-4}
$\|\Delta c\|_\infty$	47.8×10^{-2}	22.4×10^{-2}	8.0×10^{-2}
$1 - r_{\text{mass}}$	-143.4×10^{-4}	-29.1×10^{-4}	-4.9×10^{-4}
$1 - c_{\max}$	47.7×10^{-2}	22.3×10^{-2}	8.0×10^{-2}
$c_{\min}$	-2.8×10^{-4}	-2.1×10^{-6}	-1.7×10^{-8}
$r_{\text{CPU-time}}$	2.7	2.4	2.4
CPU-time (sec), limited $\kappa = \frac{1}{3}$-scheme	0.9	6.0	44.5
CPU-time (sec), benchmark problem	.	2.0	.

5.3 Diffusion

For simplicity, the equation to be considered is the 1-D advection-diffusion case of (5.1), with $f(c)$ according to (5.8) again:

$$\frac{\partial c}{\partial t} + u\frac{\partial c}{\partial x} - D\frac{\partial^2 c}{\partial x^2} = 0. \tag{5.22}$$

To still allow solutions with discontinuities, we also discretize (5.22) in its integral form. This yields the general finite-volume equation

$$\int_{\Omega_i} \frac{\partial c}{\partial t} dx + u(c_{i+\frac{1}{2}} - c_{i-\frac{1}{2}}) - D\left(\left(\frac{\partial c}{\partial x}\right)_{i+\frac{1}{2}} - \left(\frac{\partial c}{\partial x}\right)_{i-\frac{1}{2}}\right) = 0, \tag{5.23}$$

where the half-integer indices refer again to cell faces (Figure 5.1). The form (5.23) requires an evaluation of both an advective and a diffusive flux at each cell face. We proceed by re-investigating the evaluation of the advective fluxes, given a standard evaluation of the diffusive fluxes.

5.3.1 Accuracy

For the diffusive flux, the gradient $\left(\frac{\partial c}{\partial x}\right)_{i+\frac{1}{2}}$ is evaluated in the standard, $\mathcal{O}(h^2)$ central-difference manner:

$$\left(\frac{\partial c}{\partial x}\right)_{i+\frac{1}{2}} = \frac{c_{i+1} - c_i}{h}. \tag{5.24}$$

With the non-limited κ-scheme for the advective fluxes, and this central scheme for the diffusive fluxes, the following modified equation can then be derived:

$$\frac{\partial c}{\partial t} + u\frac{\partial c}{\partial x} - D\frac{\partial^2 c}{\partial x^2} + \frac{1}{24}h^2\frac{\partial^3 c}{\partial t \partial x^2} + h^2\left(\frac{\kappa - \frac{1}{3}}{4}u\frac{\partial^3 c}{\partial x^3} - \frac{1}{12}D\frac{\partial^4 c}{\partial x^4}\right) = \mathcal{O}(h^3). \tag{5.25}$$

From (5.25) it follows that for steady problems,

$$\kappa = \frac{1}{3}\left(1 + \frac{D}{u}\frac{\partial^4 c}{\partial x^4}\Big/\frac{\partial^3 c}{\partial x^3}\right) \tag{5.26}$$

is optimal. So, formally, with the $\mathcal{O}(h^2)$ gradient evaluation (5.24), the discretization of a steady advection-diffusion equation can be made $\mathcal{O}(h^3)$ by taking κ diffusion- and solution-dependent according to (5.26). This κ is such that it makes the discretization errors due to advection and diffusion cancel, under the constraint that the ratio $\frac{\partial^4 c}{\partial x^4}/\frac{\partial^3 c}{\partial x^3}$ can be evaluated sufficiently accurate. Drawbacks of this κ are its relative complexity and its expected inefficiency (particularly for complicated flux functions). Given these drawbacks and given the general dominance of advection over diffusion, we simply neglect the above diffusion- and solution-dependence of κ, which leads us to $\kappa = \frac{1}{3}$ for both steady and unsteady advection-diffusion problems.

Central difference formula (5.24) can be applied at all cell faces except those coinciding with domain boundaries. At the inflow boundary (Figure 5.2a) we apply the biased, second-order accurate difference formula

$$\left(\frac{\partial c}{\partial x}\right)_{\frac{1}{2}} = \frac{-8c_{\frac{1}{2}} + 9c_1 - c_2}{3h}, \tag{5.27a}$$

and likewise at the outflow boundary (Figure 5.2b):

$$\left(\frac{\partial c}{\partial x}\right)_{n+\frac{1}{2}} = \frac{8c_{n+\frac{1}{2}} - 9c_n + c_{n-1}}{3h}. \tag{5.27b}$$

In here, the states $c_{\frac{1}{2}}$ and $c_{n+\frac{1}{2}}$ are assumed to be prescribed by Dirichlet boundary conditions:

$$c_{\frac{1}{2}} = c_{\text{in}}, \tag{5.28a}$$

$$c_{n+\frac{1}{2}} = c_{\text{out}}. \tag{5.28b}$$

We remark that in evaluating the advective outlet flux $uc_{n+\frac{1}{2}}$ we still take (5.11e) and *not* (5.28b). This split evaluation of $c_{n+\frac{1}{2}}$ for advective and diffusive fluxes allows a continuous transition from advection-diffusion problems to pure advection problems. We proceed by analyzing the order of accuracy in the cells Ω_1 and Ω_n. Given the earlier found modified equations (5.12a) and (5.12c), and given (5.27a) and (5.27b), for the finite-volume equations

$$\int_{\Omega_1} \frac{\partial c}{\partial t} dx + u\left(c_{\frac{3}{2}} - c_{\frac{1}{2}}\right) - D\left(\left(\frac{\partial c}{\partial x}\right)_{\frac{3}{2}} - \left(\frac{\partial c}{\partial x}\right)_{\frac{1}{2}}\right) = 0, \tag{5.29a}$$

$$\int_{\Omega_n} \frac{\partial c}{\partial t} dx + u\left(c_{n+\frac{1}{2}} - c_{n-\frac{1}{2}}\right) - D\left(\left(\frac{\partial c}{\partial x}\right)_{n+\frac{1}{2}} - \left(\frac{\partial c}{\partial x}\right)_{n-\frac{1}{2}}\right) = 0, \tag{5.29b}$$

we find as corresponding modified equations, assuming smoothness of the local solutions:

$$\left(\frac{\partial c}{\partial t} + u\frac{\partial c}{\partial x} - D\frac{\partial^2 c}{\partial x^2} + h\left(\frac{1}{8}u\frac{\partial^2 c}{\partial x^2} - \frac{1}{6}D\frac{\partial^3 c}{\partial x^3}\right)\right)_1 = \mathcal{O}(h^2), \tag{5.30a}$$

$$\left(\frac{\partial c}{\partial t} + u\frac{\partial c}{\partial x} - D\frac{\partial^2 c}{\partial x^2} + h\left(-\frac{1}{3}u\frac{\partial^2 c}{\partial x^2} + \frac{1}{6}D\frac{\partial^3 c}{\partial x^3}\right)\right)_n = \mathcal{O}(h^2). \tag{5.30b}$$

So, with (5.27a) and (5.27b), we have maintained first-order accuracy in the cells Ω_1 and Ω_n. (Note that the order of accuracy in Ω_1 and Ω_n would have been reduced to zeroth-order in case of first-order difference formulae for $\left(\frac{\partial c}{\partial x}\right)_{\frac{1}{2}}$ and $\left(\frac{\partial c}{\partial x}\right)_{n+\frac{1}{2}}$.)

5.3.2 Monotonicity

In the presence of physical diffusion, besides accuracy, also monotonicity can be re-investigated. Due to physical diffusion, the amount of limiting introduced in Section 5.2.2 can be reduced. This idea and its implementation are not new; see e.g. [19]. However, just as with the aforementioned diffusion- and solution-dependent κ-relation (5.26): sacrificing much simplicity, the gain may only be a marginally improved accuracy. Therefore, we also do not change our monotonicity tools, i.e., for the discretization of advection we still apply the limited $\kappa = \frac{1}{3}$-scheme, with the limiter according to (5.17).

5.3.3 Numerical results

The present advection-diffusion discretization is applied to Problem 1. A sequence of increasingly finer grids is considered, starting off with $h = \frac{1}{20}, \frac{1}{40}, \frac{1}{80}$. For time integration - again - the explicit, fourth-order accurate, four-stage Runge-Kutta scheme is

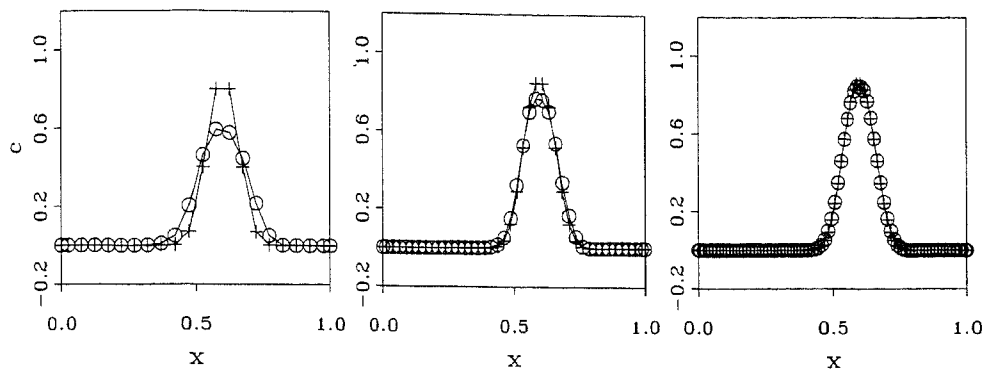

a. $h = \frac{1}{20}$. b. $h = \frac{1}{40}$. c. $h = \frac{1}{80}$.

Figure 5.9: Solutions Problem 1; ○: numerical, +: exact

Table 5.4: Numerical results Problem 1

	$h = \frac{1}{10}$	$h = \frac{1}{20}$	$h = \frac{1}{40}$	$h = \frac{1}{160}$	$h = \frac{1}{320}$
$\|\Delta c\|_1$	46.3×10^{-3}	11.5×10^{-3}	1.6×10^{-3}	2.1×10^{-4}	2.8×10^{-5}
$\|\Delta c\|_\infty$	22.3×10^{-2}	8.6×10^{-2}	1.7×10^{-2}	2.7×10^{-3}	3.8×10^{-4}

applied, with the time step - because of the dominance of advection over diffusion - simply linearly proportional to the mesh size, and sufficiently small to ensure that time discretization errors are negligible with respect to space discretization errors. (Stability and monotonicity are supposed to be guaranteed again for this small time step.)

In Figure 5.9, numerical solutions are depicted and in Table 5.4 further numerical data are given. For the grids considered, the accuracy behavior is clearly higher-order; both $\|\Delta c\|_1$ and $\|\Delta c\|_\infty$ converge like $\mathcal{O}(h^3)$. For the additional results obtained with $h = \frac{1}{160}$ and $h = \frac{1}{320}$, this is still the case (Table 5.4). The non-differentiability which is present at two points in the initial solution, does not do any harm yet.

5.4 Source terms

5.4.1 Consistent source term evaluation

Here as well, the equation to be considered is the 1-D case of (5.1) with $f(c)$ according to (5.8):

$$\frac{\partial c}{\partial t} + u\frac{\partial c}{\partial x} - D\frac{\partial^2 c}{\partial x^2} = S(x). \tag{5.31}$$

The corresponding general finite-volume equation reads

$$\int_{\Omega_i} \frac{\partial c}{\partial t} dx + \left(c_{i+\frac{1}{2}} - c_{i-\frac{1}{2}}\right) - D\left(\left(\frac{\partial c}{\partial x}\right)_{i+\frac{1}{2}} - \left(\frac{\partial c}{\partial x}\right)_{i-\frac{1}{2}}\right) = \int_{\Omega_i} S(x)dx. \tag{5.32}$$

The source term may be properly evaluated as an integrated average over cell Ω_i, or even simpler (as we would do here), as the point value in x_i. However, in case of *steady* pure advection problems with source term, both of these two straightforward source term

evaluations might cause difficulties to converge to steady state. To explain this, consider the unsteady, 1-D equation

$$\frac{\partial c}{\partial t} + u\frac{\partial c}{\partial x} = S(x), \tag{5.33a}$$

some initial solution

$$c_0 = c(x, t = 0) \in C^1, \tag{5.33b}$$

and the hypothetical source term

$$S(x) = S(c_0) \equiv u\frac{\partial c_0}{\partial x}. \tag{5.33c}$$

Then, the solution of (5.33a)-(5.33c) must be steady of course, since by definition (5.33c), the problem simplifies to

$$\frac{\partial c}{\partial t} = 0. \tag{5.34}$$

It is obvious that in a finite-volume discretization of (5.33a)-(5.33c), evaluation of $\int_{\Omega_i} S(x)dx$ in both aforementioned, straightforward ways will, due to discretization errors, in general lead to $\left(\frac{\partial c}{\partial t}\right)_i \neq 0$, $\forall i$. For higher-order accurate advection discretizations, which have little or no damping, these local errors $\left(\frac{\partial c}{\partial t}\right)_i \neq 0$ may slow down convergence to steady state. As a remedy to this, the discretization of the source term should be consistent with that of the advection operator. For this purpose we introduce the source term integral

$$\mathbf{S}(x) \equiv \frac{1}{u}\int S(x)dx, \tag{5.35}$$

and next rewrite (5.33a) as

$$\frac{\partial c}{\partial t} + u\frac{\partial}{\partial x}(c - \mathbf{S}) = 0. \tag{5.36}$$

Consider now again the hypothetical source term $S(x)$ according to (5.33c). When discretizing equation (5.36) for this hypothetical source term, convergence to steady state is guaranteed for any advection discretization for which the solver is convergent.

In case of diffusion, we maintain this approach; i.e., instead of (5.31) we consider

$$\frac{\partial c}{\partial t} + u\frac{\partial c}{\partial x}(c - \mathbf{S}) - D\frac{\partial^2 c}{\partial x^2} = 0, \tag{5.37}$$

with $\mathbf{S} = \mathbf{S}(x)$ still according to (5.35). Next of (5.37) we take the integral form, which in cell Ω_i leads to the equation

$$\int_{\Omega_i}\frac{\partial c}{\partial t}dx + u\left(\left(c_{i+\frac{1}{2}} - \mathbf{S}_{i+\frac{1}{2}}\right) - \left(c_{i-\frac{1}{2}} - \mathbf{S}_{i-\frac{1}{2}}\right)\right) - D\left(\left(\frac{\partial c}{\partial x}\right)_{i+\frac{1}{2}} - \left(\frac{\partial c}{\partial x}\right)_{i-\frac{1}{2}}\right) = 0. \tag{5.38}$$

The extended advective flux $u\left(c_{i+\frac{1}{2}} - \mathbf{S}_{i+\frac{1}{2}}\right)$ can be evaluated in one's own favorite manner. Here, we apply the limited $\kappa = \frac{1}{3}$-scheme:

$$\begin{aligned}\left(c_{i+\frac{1}{2}} - \mathbf{S}_{i+\frac{1}{2}}\right) &= (c_i - \mathbf{S}_i) + \frac{1}{2}\phi(r_{i+\frac{1}{2}})\left((c_i - \mathbf{S}_i) - (c_{i-1} - \mathbf{S}_{i-1})\right), \\ r_{i+\frac{1}{2}} &= \frac{(c_{i+1} - \mathbf{S}_{i+1}) - (c_i - \mathbf{S}_i) + \epsilon}{(c_i - \mathbf{S}_i) - (c_{i-1} - \mathbf{S}_{i-1}) + \epsilon},\end{aligned} \tag{5.39}$$

in which the limiter function $\phi(r)$ is again according to (5.17). Because it is steady, the source term by no means influences the propagation direction of c, and hence neither the upwinding direction.

5.4.2 Numerical results

To investigate the merits of the proposed, consistent source term evaluation, numerical results are presented for Problem 2; the problem with the source term

$$\begin{array}{ll} S(x) = \frac{\pi}{b-a} u \sin\left(2\pi\frac{x-a}{b-a}\right) - \frac{2\pi^2}{(b-a)^2} D \cos\left(2\pi\frac{x-a}{b-a}\right), & x \in [a,b], \\ S(x) = 0, & x \notin [a,b]. \end{array} \tag{5.40}$$

For $D \neq 0$, the source term is discontinuous at $x = a$ and $x = b$. As a consequence, one may expect a non-differentiability in the solution at these points. If such a non-differentiability occurs, formally, the differential form (5.31) is not valid. Applying an integral form, this validity aspect is expected to be no point. In behalf of the consistent source term evaluation, the source (5.40) can be easily integrated by hand to $\mathbf{S}(x)$:

$$\begin{array}{ll} \mathbf{S}(x) = -\frac{1}{2}\cos\left(2\pi\frac{x-a}{b-a}\right) - \frac{\pi}{b-a}\frac{D}{u}\sin\left(2\pi\frac{x-a}{b-a}\right) + C_1, & x \in [a,b], \\ \mathbf{S}(x) = C_2, & x \notin [a,b], \end{array} \tag{5.41}$$

with C_1 and C_2 the integration constants. We choose $C_2 = 0$. To enhance the solution's smoothness, C_1 should be chosen such that $\mathbf{S}(x)$ inside $[a,b]$ fits continuously to $\mathbf{S}(x)$ outside $[a,b]$, which leads to $C_1 = \frac{1}{2}$. Resumingly, we have the *continuous* source integrals:

$$\begin{array}{ll} \mathbf{S}(x) = \frac{1}{2}\left(1 - \cos\left(2\pi\frac{x-a}{b-a}\right)\right) - \frac{\pi}{b-a}\frac{D}{u}\sin\left(2\pi\frac{x-a}{b-a}\right), & x \in [a,b], \\ \mathbf{S}(x) = 0, & x \notin [a,b]. \end{array} \tag{5.42}$$

Given our use of equations in integral form, the above continuity condition applied in deriving $\mathbf{S}(x)$ is in fact not a necessity. E.g., we could also have taken $C_1 = C_2 = 0$, leading to the *discontinuous* source integrals

$$\begin{array}{ll} \mathbf{S}(x) = -\frac{1}{2}\cos\left(2\pi\frac{x-a}{b-a}\right) - \frac{\pi}{b-a}\frac{D}{u}\sin\left(2\pi\frac{x-a}{b-a}\right), & x \in [a,b], \\ \mathbf{S}(x) = 0, & x \notin [a,b]. \end{array} \tag{5.43}$$

Numerical experiments are performed again on a sequence of three grids with $h = \frac{1}{20}, \frac{1}{40}$ and $\frac{1}{80}$. To converge to steady state, we also apply the explicit, fourth-order accurate, four-stage Runge-Kutta scheme, with the time step again linearly proportional to the mesh size. (No effort is put in implementation of an efficient steady-state solver.) As the initial solution, in all cases we take $c(x) = 0$. We start by considering the pure advection case $D = 0$. For the point-wise cell-centered, straightforward source term evaluation, residual convergence is slow indeed (Figure 5.10). Applying the consistent source term evaluation (with the continuously fitted integrals (5.42)), residual convergence is faster and also more regular (Figure 5.10). Moreover, the accuracy of the corresponding numerical solutions is remarkable; on each of the three grids the exact solution is obtained (Figure 5.11). Of course, this is sheer coincidence; for $D = 0$, $\mathbf{S}(x)$ according to (5.42), is identical to the exact solution:

$$\begin{array}{ll} c(x) = \frac{1}{2}\left(1 - \cos\left(2\pi\frac{x-a}{b-a}\right)\right), & x \in [a,b], \\ c(x) = 0, & x \notin [a,b]. \end{array} \tag{5.44}$$

Hence, at convergence to steady state, in (5.38) we have exact cancelling of space discretization errors. A funny consequence of this exact cancelling is that the advection

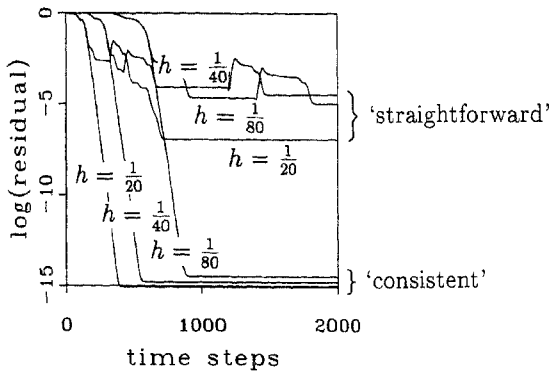

Figure 5.10: Convergence histories Problem 2, $D = 0$. (Straightforward source term evaluation slows down convergence to steady state.)

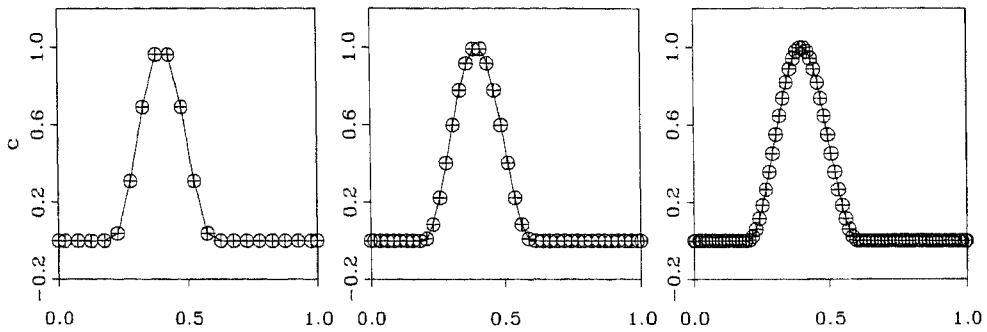

a. $h = \frac{1}{20}$. b. $h = \frac{1}{40}$. c. $h = \frac{1}{80}$.

Figure 5.11: Solutions Problem 2, $D = 0$; $\circ$: numerical (consistent source term evaluation), $+$: exact. (Numerical solutions are exact.)

Table 5.5: Numerical results Problem 2, $D = 0.01$.

	$h = \frac{1}{20}$	$h = \frac{1}{40}$	$h = \frac{1}{80}$
$\|\Delta c\|_1$	106.2×10^{-4}	19.3×10^{-4}	4.0×10^{-4}
$\|\Delta c\|_\infty$	51.0×10^{-3}	10.1×10^{-3}	2.6×10^{-3}

a. Straightforward source term evaluation

	$h = \frac{1}{20}$	$h = \frac{1}{40}$	$h = \frac{1}{80}$
$\|\Delta c\|_1$	20.2×10^{-4}	4.2×10^{-4}	1.1×10^{-4}
$\|\Delta c\|_\infty$	8.1×10^{-3}	2.4×10^{-3}	1.1×10^{-3}

b. Consistent source term evaluation

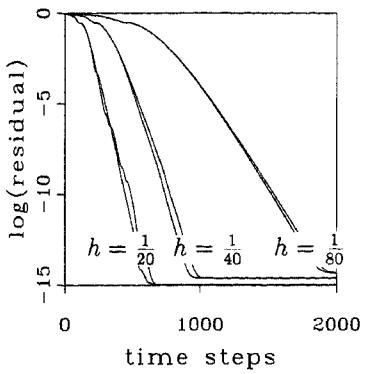

Figure 5.12: Convergence histories Problem 2, $D = 0.01$. (No significant differences in convergence rates between straightforward and consistent source term evaluation.)

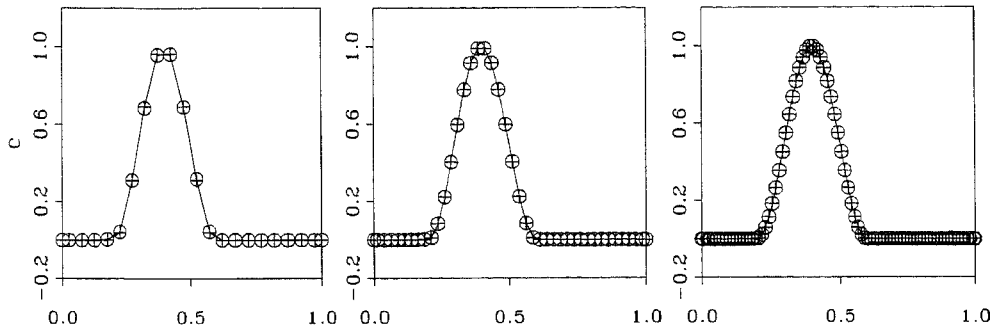

a. $h = \frac{1}{20}$. b. $h = \frac{1}{40}$. c. $h = \frac{1}{80}$.

Figure 5.13: Solutions Problem 2, $D = 0.01$; ○: numerical (consistent source term evaluation), +: exact

discretization does not play a role any more. E.g., in evaluating the extended advective fluxes we could have replaced the limited $\kappa = \frac{1}{3}$-scheme by the first-order accurate upwind scheme, without loss of the exact resolution.

For the prescribed diffusive test case, $D = 0.01$, as opposed to the $D = 0$-case, the results of the straightforward source term evaluation are satisfactory. On all three grids, the straightforward discretization leads to practically the same residual convergence rates as the consistent method (Figure 5.12). Further, there appears to be second-order accuracy behavior with respect to $\|\Delta c\|_1$ (Table 5.5a). The convergence of $\|\Delta c\|_\infty$ is still close to $\mathcal{O}(h^2)$, but is probably diminishing to $\mathcal{O}(h)$ for further decreasing h. The solution errors corresponding to the consistent source term evaluation are converging less fast (Table 5.5b). Yet, when comparing error levels in Tables 5.5a and 5.5b, the consistent source term evaluation is still to be preferred; on all three grids it yields smaller errors, both in L_1- and L_∞-norm. In Figure 5.13 we give graphs of the numerical solutions obtained by the consistent method. Particularly note the very good accuracy on the coarsest grid (Figure 5.13a).

To finish, we still show the ability of the consistent discretization to capture much

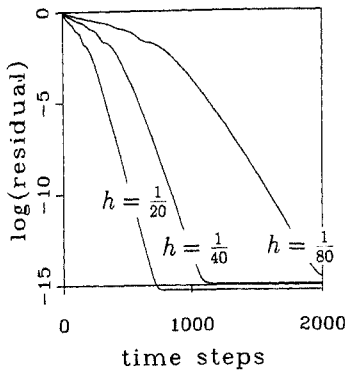

Figure 5.14: Convergence histories Problem 2, $D = 0.01$, *discontinuous source integrals*; consistent source term evaluation

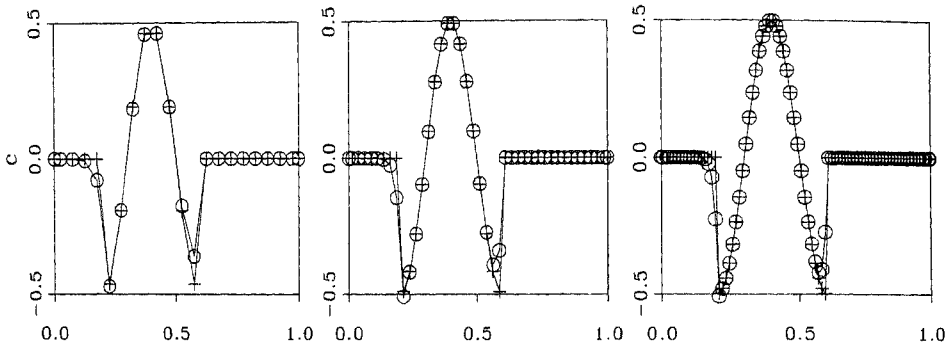

a. $h = \frac{1}{20}$. b. $h = \frac{1}{40}$. c. $h = \frac{1}{80}$.

Figure 5.15: Solutions Problem 2, $D = 0.01$, *discontinuous source integrals*; ○: numerical (consistent source term evaluation), +: exact

less differentiable solutions. For this, note that the integral form of (5.31) formally has exact solutions of the type

$$\begin{aligned} c(x) &= -\tfrac{1}{2}\cos\left(2\pi\tfrac{x-a}{b-a}\right) + C, \qquad && x \in [a,b], \\ c(x) &= 0, && x \notin [a,b], \end{aligned} \tag{5.45}$$

with C an arbitrary constant. (The method with straightforward source term evaluation does not allow this general class of solutions (5.45), but only the continuous solution (5.44); i.e. (5.45) with $C = \frac{1}{2}$.) Taking the discontinuous case $C = 0$ and the corresponding discontinuous pair of source term integrals (5.43), with the consistent source term evaluation we get the numerical results given in Figures 5.14 and 5.15.

5.5 Conclusions

- The present limited $\kappa = \frac{1}{3}$-discretization of the advection operator appears to be a satisfactory method, not solely for problems with discontinuities, but also for smoother problems. It has been applied to all present test problems, without difficulty and without any modification. The novel limiter works well.
- Application of the simple, directionally-split, 1-D upwind approach to the present multi-D advection problem (Problem 4), has not led to unsatisfactory results. 'Genuinely' multi-D upwinding is not always necessary.
- An advantage of the present discretization of advection-diffusion operators, is that it does not impose an upper bound to the diffusion coefficient D, above which the discretization is no longer sensitive to variations in D, or no longer stable. Starting from any low, practically relevant value of D, an accurate and smooth transition to pure advection is possible.
- The proposed consistent discretization of advection-diffusion equations with source terms, is interesting for reasons of both accuracy and convergence to steady state. The more dominant advection over diffusion, the more this holds. The drawback of the additional task to integrate the source term is not so serious, given the ample, present-day availability of well-developed computer algebra software. Of course, in case of source terms already given in differential form (say as $\frac{\partial S}{\partial x}$), this additional integration task does not even need to be performed.
- Beside its accuracy and efficiency properties, the conservation and monotonicity properties of the complete discretization method are satisfactory as well. Possibly severe requirements imposed in e.g. environmental transport computations, probably can all be satisfied.
- In our opinion, the main advantage of the complete discretization method is that it is robust; without any tuning, it works satisfactory for all kinds of advection-diffusion problems.

Acknowledgment

Jan van Eijkeren and Fred Walsteijn are acknowledged for their suggestions in improving this chapter.

References

[1] BOLLEY, C., CROUZEIX, M.: Conservation de la positivité lors de la discrétisation des problèmes d'évolution paraboliques, *RAIRO Analyse Numérique/Numerical Analysis*, **12** (1978), pp. 237-245.

[2] GODUNOV, S.K.: Finite difference method for numerical computation of discontinuous solutions of the equations of fluid dynamics, (Cornell Aeronautical Lab. Transl. from the Russian) *Math. Sbornik*, **47** (1959), pp. 271-306.

[3] HEMKER, P.W.: Defect correction and higher order schemes for the multi grid solution of the steady Euler equations, *Lecture Notes in Mathematics*, **1228** (Springer-Verlag, Berlin, 1986), pp. 149-165.

[4] KOREN, B.: Defect correction and multigrid for an efficient and accurate computation of airfoil flows, *J. Comput. Phys.*, **77** (1988), pp. 183-206.

[5] —: Upwind discretization of the steady Navier-Stokes equations, *Int. J. Numer. Meth. Fluids*, **11** (1990), pp. 99-117.

[6] —, HEMKER, P.W.: Multi-D upwinding and multigridding for steady Euler flow computations, *Notes on Numerical Fluid Mechanics*, **35** (Vieweg, Braunschweig, 1992), pp. 89-98.

[7] —, VAN DER MAAREL, H.T.M.: Monotone, higher-order accurate multi-dimensional upwinding, *Lecture Notes in Physics*, **414** (Springer-Verlag, Berlin, 1993), pp. 110-114.

[8] KRAAIJEVANGER, J.F.B.M.: Contractivity of Runge-Kutta methods, *BIT*, **31** (1991), pp. 482-528.

[9] LAX, P.D.: Hyperbolic systems of conservation laws II, *Comm. Pure Appl. Math.*, **10** (1957), pp. 537-566.

[10] VAN LEER, B.: Upwind-difference methods for aerodynamic problems governed by the Euler equations, *Lectures in Applied Mathematics*, **22 – Part 2** (American Mathematical Society, Providence, RI, 1985), pp. 327-336.

[11] LEVEQUE, R.J.: *Numerical Methods for Conservation Laws* (Birkhäuser, Basel, 1990).

[12] PATANKAR, S.V.: *Numerical Heat Transfer and Fluid Flow* (Hemisphere, New York, 1980).

[13] SANZ-SERNA, J.M., VERWER, J.G., HUNDSDORFER, W.H.: Convergence and order reduction of Runge-Kutta schemes applied to evolutionary problems in partial differential equations, *Numer. Math.*, **50** (1987), pp. 405-418.

[14] SHU, C.-W., OSHER, S.: Efficient implementation of essentially non-oscillatory shock-capturing schemes, *J. Comput. Phys.*, **77** (1988), pp. 439-471.

[15] SHU, C.-W., OSHER, S.: Efficient implementation of essentially non-oscillatory shock-capturing schemes II, *J. Comput. Phys.*, **83** (1989), pp. 32-78.

[16] SPEKREIJSE, S.P.: Multigrid solution of monotone second-order discretizations of hyperbolic conservation laws, *Math. Comput.*, **49** (1987), pp. 135-155.

[17] SPIJKER, M.N.: Contractivity in the numerical solution of initial value problems, *Numer. Math.*, **42** (1983), pp. 271-290.

[18] SWEBY, P.K.: High resolution schemes using flux limiters for hyperbolic conservation laws, *SIAM J. Numer. Anal.*, **21** (1984), pp. 995-1011.

[19] TORO, E.F.: Viscous flux limiters, *Notes on Numerical Fluid Mechanics*, **35** (Vieweg, Braunschweig, 1992), pp. 592-600.